https://doi.org/10.1016/j.euromechflu.2019.04.010

Numerical simulation of fiber conveyance in a confined channel by the immersed boundary-lattice Boltzmann method

Jingyu Cui[1,3], Zhe Lin[1,2], Yuzhen Jin*[1,2], Yang Liu[3]

1. Faculty of Mechanical Engineering & Automation, Zhejiang Sci-Tech University, Hangzhou, Zhejiang Province, China.
2. State-Province Joint Engineering Lab of Fluid Transmission System Technology, Hangzhou, Zhejiang Province, China
3. Department of Mechanical Engineering, The Hong Kong Polytechnic University, Hung Hom, Hong Kong, China

Abstract

Fluid-structure interaction (FSI) phenomenon is very common in pneumatic-type textile field. However, the motion of flexible bodies, for instance, fibers or yarns, are usually difficult to simulate due to their large fineness ratio and high flexibility. Conventional FSI solvers based on the body-fitted grid method are difficult to handle the large deformation due to severe grid distortion. In this paper, we studied the fluid-fiber interaction for fiber conveyance in a fiber transport channel (FTC) using the immersed boundary-lattice Boltzmann method (IB-LBM). The effect of three parameters on fiber conveyance, i.e. the conical degree of the FTC ($\tan\alpha$), the bending rigidity of fiber ($\widehat{K}_b$) and the flow Reynolds number (Re), are particularly investigated. The calculated results indicate that the converging shape of FTC helps to straighten fiber and adjust its orientation to a more horizontal degree during the conveyance, however, it may not improve fiber delivery efficiency, and a larger conical degree brings a better straighten effect and a smaller leading angle if fiber-wall contact does not occur. Under the conditions that $\tan\alpha > 0$, $Re < 400$ and $\widehat{K}_b < 1e-3$, the straightness undergoes a "leap-slump-grow-drop" evolution process and the leading angle follows an "increase-decline" tendency. Moreover, the simulation results show that the bending rigidity have a significant effect on fiber configuration and orientation during its conveyance, and a fiber with a larger bending rigidity is more likely to maintain a straighter configuration and a more horizontal orientation during its conveyance. As Re increases in simulations, the fiber gets less straight

in configuration and more vertical in orientation, and deviates more from the horizontal path.

Key words: Fluid-structure interaction; Fiber conveyance; Immersed boundary method; lattice Boltzmann method;

1. Introduction

Fiber conveyance is quite common in pneumatic-type textile field, and the way how it carries out by the fluid may be essential to the qualities of the final spun yarn. For example, in rotor spinning, the strength of rotor spun yarns can be well improved by optimizing the fiber conveyance in fiber transfer channel (FTC), which increases the proportion of straight fibers within rotor spun yarns [1-3]. Driven by the purpose of improving yarn quality, numerical studies on the fiber conveyance in FTC have been performed [4-6], however, the underlying physical mechanism of the motion of the fiber in the flow is still not fully understood. The problem of fibers' transportation in confined channel is a complex fluid-structure-interaction (FSI) problem. The high flexibility and elasticity of the fiber may cause large deformation and displacement during simulation, which complicates the conventional body-fitted grid based FSI solvers and results in expensive computation cost. Therefore, it is rather demanding to develop a more practical method to solving FSI problems involving large deformation and displacement at low computational cost.

The immersed boundary method (IBM) is a very powerful numerical approach for different problems involving interaction between fluids and elastic structures. It is originally developed by Peskin [7-9] for simulating the blood flow in human heart and dynamics of heart valves, and then widely used in the area of computational biofluid mechanics, such as simulation of red blood cells deformation [10], swimming motion of creatures such as sperm [11] and eel [12] and flight motion of an insect [13]. The method is based on the non-body-fitted Cartesian grid, i.e., the fluid is represented on an Eulerian coordinate and the structure is represented on a Lagrangian coordinate, and the presence of solid boundaries is modelled by a body force term in the flow equations hence no extra effort is necessary to alter the underlying computational grid. These features make IBM a competitive method to deal with complex moving geometries efficiently.

On the other hand, the lattice-Boltzmann method (LBM) is an alternative and robust method for solving fluid mechanics problems, and has drawn tremendous attention in last two decades. Different from conventional macro-derived approach, the LBM starts from a perspective of mesoscopic and deals with a single-particle velocity distribution function that obeys an approximate Boltzmann equation. The macro physical quantities, such as density, velocity, and pressure, can be obtained through statistics. It has been well proved in the past few decades that the LBM possesses a great capability in simulating fluid physics [14].

In recent years, there has been an increasing interest in combining LBM and IBM to solve FSI problems, as represented by the problem of flow around flexible slender objects such as fiber and elastic filament. Vahidkhah and Abdollahi [15] simulated the interactions of a flexible fiber with a viscous incompressible fluid by IB-LBM. In their simulation the fiber was tethered in one end initially with a fixed angle to the coming flow and the deformation of the fiber was particularly analyzed. Tian et al. [16] proposed a modified penalty approach-based IB-LBM to model an incompressible flow coupling with elastic filaments with finite mass. In their approach, the inertial force of the thin solid structure was incorporated by connecting this structure through virtual springs to a ghost structure with the equivalent mass. The solver had been proved to be numerically stable and quite efficient, and their study on the elastic filament flapping might offer a physical insight to the biological behavior of the fish. Yuan et al. [17] numerically studied the flapping and trajectory of filament (a single and a pair respectively) with the upstream end fixed in a uniform flow by a momentum exchanged-based IB-LBM. Their numerical results qualitatively well agree with the experimental results of Zhang et al. [18].

Study on the motion and transient configuration of the fiber during its conveyance is a typical FSI problem and is of engineering significance to the quality and efficiency improvement of yarn. The development of IB-LBM has made it quite powerful in handling this type of FSI problem. In this paper, we used IB-LBM to simulate fiber conveyance in the FTC, in which the fiber configuration's evolution during the conveyance is particularly focused. Moreover, the effects of the conical degree of FTC, the bending rigidity of fiber and the flow Reynolds number (Re) on fiber's configuration and motion pattern are investigated, and two parameters $\emptyset$ and θ are proposed to characterize and analyze the straightness and orientation of the fiber during

its conveyance in FTC.

2. Mathematic formulation and numerical method

2.1 Fiber model and its equation of motion

The slender fiber is represented by a set of equally spaced isometric Lagrangian points $\vec{X}(\mathrm{s}_i, \mathrm{t}),\ \ \mathrm{i} = 0, 1, \cdots, Nb,$ as demonstrated in Fig.1. The length of the divided fiber segment in equilibrium state is Δs. When subjected a flow-induced force, those Lagrangian points move according to Newton's law. The fiber is delivered by the fluid drag and its shape is altered by bending and stretching.

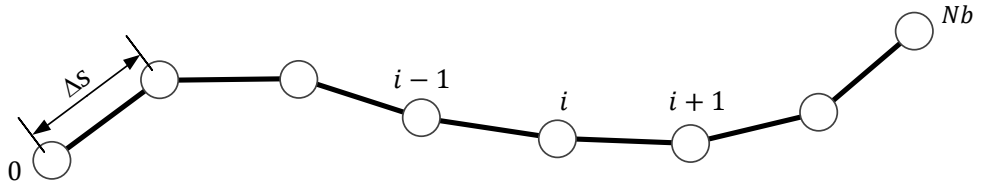

Fig.1. Fiber model adopted in our current simulation

By assuming a uniform mass distribution along the length of fiber (i.e. a constant linear density ρ_s) and ignores the influence of gravity and buoyance, the nonlinear fiber motion in fluid flow can be described by

$$\rho_s \frac{\partial^2 \vec{X}}{\partial t^2} = \vec{F}_s + \vec{F}_b + \vec{F}_{fluid} \tag{1}$$

which can be further expressed as[19, 20]

$$\rho_s \frac{\partial^2 \vec{X}}{\partial t^2} = \frac{\partial}{\partial s}\left[T(s)\frac{\partial \vec{\mathrm{X}}}{\partial \mathrm{s}}\right] - K_b \frac{\partial^4 \vec{X}}{\partial s^4} + \vec{F}_{fluid} \tag{2}$$

with the tensile force

$$T(s) = K_s\left(\left(\frac{\partial \vec{\mathrm{X}}}{\partial \mathrm{s}} \cdot \frac{\partial \vec{\mathrm{X}}}{\partial s}\right)^{\frac{1}{2}} - 1\right) \tag{3}$$

here $\vec{X}$ is the position vector of the fiber node, the term $\rho_s \frac{\partial^2 \vec{X}}{\partial t^2}$ is the inertial force, $\vec{F}_s$, $\vec{F}_b$ and $\vec{F}_{fluid}$ are three forces exerting on the fiber node, i.e. stretching force (further calculated use the term $\frac{\partial}{\partial s}\left[T(s)\frac{\partial \vec{X}}{\partial \mathrm{s}}\right]$), bending force (further calculated use the term $-K_b \frac{\partial^4 \vec{X}}{\partial s^4}$) and hydrodynamic force from the fluid, respectively. s is the Lagrangian coordinate along the length. The linear density ρ_s, stretching coefficient K_s and bending rigidity K_b are 3 parameters

used to describe the structural properties of the fiber.

The right-hand side of Equation (2) can be solved explicitly using a central difference scheme.

$$m_s \frac{\partial^2 \vec{X}}{\partial t^2} = \vec{F}_j(\vec{\mathrm{X}}, t) + \frac{T_{i+\frac{1}{2}}\left[\frac{\partial \vec{X}}{\partial \mathrm{s}}\right]_{i+\frac{1}{2}} - T_{i-\frac{1}{2}}\left[\frac{\partial \vec{X}}{\partial \mathrm{s}}\right]_{i-\frac{1}{2}}}{\Delta s} - K_b \frac{\vec{X}_{i+2} - 4\vec{X}_{i+1} + 6\vec{X}_i - 4\vec{X}_{i-2} + \vec{X}_{i-2}}{\Delta s^4} \tag{4}$$

where $\frac{\partial \vec{X}}{\partial \mathrm{s}}$ is the tangent vector which can be calculated at the segment center $i + \frac{1}{2}$ via first order central difference scheme

$$\left[\frac{\partial \vec{X}}{\partial \mathrm{s}}\right]_{i+\frac{1}{2}} = \frac{\vec{X}_{i+1} - \vec{X}_i}{\Delta s}, \text{ and } \left[\frac{\partial \vec{X}}{\partial \mathrm{s}}\right]_{i-\frac{1}{2}} = \frac{\vec{X}_i - \vec{X}_{i-1}}{\Delta s} \tag{5}$$

and the tension force $T_{i+\frac{1}{2}}$ is calculated by the equation

$$T_{i+\frac{1}{2}} = K_s\left(\left|\frac{\vec{X}_{i+1} - \vec{X}_i}{\Delta s}\right| - 1\right), \text{and } T_{i-\frac{1}{2}} = K_s\left(\left|\frac{\vec{X}_i - \vec{X}_{i-1}}{\Delta s}\right| - 1\right) \tag{5}$$

2.2 Flow field solver -Lattice Boltzmann method

In present simulations, a lattice Boltzmann method with a single relaxation time (SRT) and a two-dimensional model with nine speeds (D2Q9) is used to solve the flow field. The dimensionless lattice Boltzmann equation with BGK approximation under an external force is given as follows,

$$f_j\left(\vec{x} + \vec{e}_j \Delta t, t + \Delta t\right) = f_j(\vec{x}, t) - \frac{1}{\tau}\left(f_j(\vec{x}, t) - f_j^{eq}(\vec{x}, t)\right) + \vec{F}_j \Delta t \tag{6}$$

With

$$\vec{F}_j = \left(1 - \frac{1}{2\tau}\right)\omega_j\left(\frac{\vec{e}_j - \vec{u}}{c_s^2} + \frac{\vec{e}_j \cdot \vec{u}}{c_s^4}\vec{e}_j\right)\vec{f}(\vec{x}, t) \tag{7}$$

where $f_j(\vec{x}, t)$ is the distribution function for particles at position $\vec{x}$ with velocity $\vec{e}_j$ at time t, $f_j^{eq}(\vec{x}, t)$ is the Maxwellian equilibrium distribution function, τ is the dimensionless relaxation time which is related to the dimensionless kinematic viscosity by the equation $\nu = c_s^2(\tau - 0.5)\Delta t$ and Δt is the time interval, $\vec{f}(\vec{x}, t)$ is the external force term exerted to the fluid by the immersed boundary, $\vec{e}_j$ is the particle velocity and ω_j are weights coefficient of D2Q9 velocity model, which is given by

$$\vec{e}_j = \begin{cases} (0,0), & j = 0 \\ \vec{c}\left(\cos\frac{\pi(j-1)}{2}, \sin\frac{\pi(j-1)}{2}\right), & j = 1,2,3,4 \\ \sqrt{2}\vec{c}\left(\cos\frac{\pi(2j-1)}{4}, \sin\frac{\pi(2j-1)}{4}\right), & j = 5,6,7,8 \end{cases} \quad (9)$$

where $\vec{c}$ is the lattice speed, whose value is defined as $c = \frac{\Delta x}{\Delta t} = 1$ in our model, and Δx is the lattice space. For an isothermal fluid, the equilibrium distribution function $f_j^{eq}(\vec{x}, t)$ in the D2Q9 model is given by the following equation as

$$f_j^{eq}(\vec{x}, t) = \omega_j \rho \left[1 + \frac{\vec{e}_j \cdot \vec{u}}{c_s^2} + \frac{(\vec{e}_j \cdot \vec{u})^2}{2c_s^4} - \frac{\vec{u}^2}{2c_s^2}\right] \quad (8)$$

where the weighting coefficient ω_j is given as: $\omega_0 = 4/9$, $\omega_{1,2,3,4} = 1/9$ and $\omega_{5,6,7,8} = 1/36$. $c_s = \frac{c}{\sqrt{3}} = \frac{1}{\sqrt{3}}$ is the sound speed, ρ and $\vec{u}$ are the macroscopic density and velocity of the fluid respectively which are computed from $f_j(\vec{x}, t)$ and the external force $\vec{f}(\vec{x}, t)$every time interval at each fluid node as follows:

$$\rho = \sum_j f_j \quad (9)$$

$$\vec{u} = \frac{1}{\rho}\left(\sum_j f_j \vec{e}_j + \frac{1}{2}\vec{f}\Delta t\right) \quad (10)$$

2.3 Interaction forces calculation- Immersed boundary method

The interaction between the fluid and the moving fiber is handled by a momentum exchange scheme-based immersed boundary method (IBM), which is proposed by Niu et al. [21] In this scheme, the distribution function on the boundary points at all velocity directions is interpolated first. In our case, we use a smooth Dirac delta function $\sigma_h()$ which is proposed by Peskin [9].

$$f_j(\vec{X}, t) = \sum_{\vec{x}} f_j(\vec{x}, t)\sigma_h(\vec{x} - \vec{X})\,\Delta x^2 \quad (11)$$

With

$$\sigma_h(\vec{x} - \vec{X}) = \frac{1}{\Delta x^2}\psi\left(\frac{x-X}{\Delta x}\right)\psi\left(\frac{y-Y}{\Delta x}\right) \quad (12)$$

$$\psi(r) = \begin{cases} \frac{1}{4}\left(1 + cos\left(\frac{\pi|r|}{2}\right)\right) & |r| \le 2 \\ 0, & \text{otherwise} \end{cases} \quad (15)$$

where Δx is the mesh spacing of the Eurerian grid and $\sum_{\vec{x}}$ is the summations over all the Eulerian grid points.

In order to satisfy the non-slip boundary condition on the fiber, a new set of distribution functions on the boundary points need be computed by using the bounce-back rules [22, 23].

$$f_{-j}(\vec{X}, t+\Delta t) = f_j(\vec{X}, t) - 2\omega_j \rho \frac{\vec{e}_j \, \vec{u}(\vec{X},t)}{c_s^2} \tag{13}$$

where $-j$ denotes the opposite direction of j, i.e., $\vec{e}_{-j} = \vec{e}_j$ and ρ is the fluid density at the boundary points. Consequently, the Lagrangian force density generated by the boundary points of the fiber can be calculated via the momentum exchange as follow,

$$\vec{g}(\vec{X}, t) = \sum_j \vec{e}_j \left[f_j(\vec{X}, t+\Delta t) - f_{-j}(\vec{X}, t) \right] \tag{14}$$

The hydrodynamic force exerted on the boundary point is the reaction force of $\vec{g}(\vec{X}, t)$,

$$\vec{F}(\vec{X}, t) = -\vec{g}(\vec{X}, t) \tag{15}$$

And further we can spread the Lagrangian force density to the surrounding fluid by Dirac delta function $\sigma_h(\,)$,

$$\vec{f}(\vec{x}, t) = \sum_{\vec{x}} \vec{e}_j \; \vec{g}(\vec{X}, t) \sigma_h(\vec{x} - \vec{X}) \Delta s \tag{16}$$

where Δs is the Lagrangian grid spacing and $\sum_{\vec{x}}$ means the summations over all the Lagrangian grid points.

2.4 Position and velocity update for fiber nodes

In order to improve the numerical stability of the algorithm, a three-step Runge–Kutta method of "Equation (20)-(25)" is applied to update the velocity $\vec{U}_i$ and position $\vec{X}_i$ of each fiber node. For each step, the acceleration $\frac{\partial^2 \vec{X}_i^n}{\partial t^2}$ is calculated explicitly using Equation (1) based on the intermediate fiber configuration ($\vec{X}_i^{(1)}, \vec{U}_i^{(1)}, \vec{X}_i^{(2)}$, and $\vec{U}_i^{(2)}$) and hydrodynamic force in previous step *n*. Implementation details are as follows:

Step 1

$$\vec{U}_i^{(1)} = \vec{U}_i^n + \Delta t \frac{\partial^2 \vec{X}_i^n}{\partial t^2} \tag{17}$$

$$\vec{X}_i^{(1)} = \vec{X}_i^n + \Delta t \vec{U}_i^n \tag{18}$$

Step 2

$$\vec{U}_i^{(2)} = \frac{3}{4}\vec{U}_i^n + \frac{1}{4}\left(\vec{U}_i^{(1)} + \Delta t \frac{\partial^2 \vec{X}_i^{(1)}}{\partial t^2} \right) \tag{19}$$

$$\vec{X}_i^{(2)} = \frac{3}{4}\vec{X}_i^n + \frac{1}{4}\left(\vec{X}_i^{(1)} + \Delta t \vec{U}_i^{(1)} \right) \tag{20}$$

Step 3

$$\vec{U}_i^{n+1} = \frac{1}{3}\vec{U}_i^n + \frac{2}{3}\left(\vec{U}_i^{(2)} + \Delta t \frac{\partial^2 \vec{X}_i^{(2)}}{\partial t^2}\right) \tag{21}$$

$$\vec{X}_i^{n+1} = \frac{1}{3}\vec{X}_i^n + \frac{2}{3}\left(\vec{X}_i^{(2)} + \Delta t \vec{U}_i^{(2)}\right) \tag{22}$$

where the superscript n is the time step index and subscript i represents the ith fiber point. Given the values of all variables at time step n, the numerical implementation process of the employed IB–LB scheme is summarized as follows:

1). Implement the collision and stream process of LBM without external force term till convergence to obtain the initial flow field.

2). Compute the density distribution functions $f_j(\vec{X}, t)$ on the boundary point in all 9 directions using Equation (13).

3). A new set of distribution functions $f_j(\vec{X}, t + \Delta t)$ on the boundary points can be obtained using bounce-back rules by Equation (16).

4). Compute the Lagrangian force density $\vec{g}(\vec{X}, t)$, and its reaction force density $\vec{F}(\vec{X}, t)$on the boundary points by Equation (17) and (18).

5). Spread the Lagrangian force density $\vec{g}(\vec{X}, t)$ on all the fluid points by Equation (19) to obtain the external force density $\vec{f}(\vec{x}, t)$.

6). Update the velocity distribution function $f_j(\vec{x} + \vec{e}_j \Delta t, t + \Delta t)$ via collision and stream process with external force term according to Equation (7) and (8).

7). Compute the macro fluid density ρ and velocity field $\vec{u}$ using Equation (11) and (12).

8). Use the three-step Runge–Kutta method of Equation (20)-(25) to update fiber point position $\vec{X}_i$ and velocity $\vec{U}_i$.

9). Repeat Steps (3) to (8) until the conveyance is achieved (for steady-flow problems), or the desired process is completed (for transient problems).

3. Validation of the numerical method

3.1 Flow over a single flexible filament with its upstream end tethered

To validate present numerical algorithm for FSI problems, flow past a flexible elastic filament with its upstream end tethered is simulated. The physical schematic and boundary

conditions are illustrated in Fig.2. The computational domain is a rectangle of $9.5L \times 3.5L$ and the filament is initially given a small sine-wave perturbation, with its upstream end simply fixed at $(L, 1.75L)$. A uniform flow with a constant velocity of u_∞ comes from the left inlet. The enlarged view placed behind the filament shows the grid details of our simulations that two sets of grids are used and grid points at the boundary do not need to coincide. In all our simulations, the quantities used are dimensionless. The filament's 3 parameters ρ_s, K_s and K_b are non-dimensionalized by the characteristic length L, characteristic velocity u_∞ and fluid density ρ_f in the following forms.

$$M = \frac{\rho_s}{\rho_f L},\ \widehat{K}_s = \frac{K_s}{\rho_f (u_\infty)^2 L},\ \widehat{K}_b = \frac{K_b}{\rho_f (u_\infty)^2 L^2} \tag{23}$$

During the simulations, the simply fixed boundary condition is applied to the upstream end of the filament:

$$\vec{X} = \vec{X}_0,\ \frac{\partial^2 \vec{X}}{\partial s^2} = 0 \tag{24}$$

and the free-end boundary condition is applied to the downstream end of the filament:

$$\frac{\partial^2 \vec{X}}{\partial s^2} = \frac{\partial^3 \vec{X}}{\partial s^3} = 0 \tag{25}$$

which means the bending moment and the transverse stress vanishes.

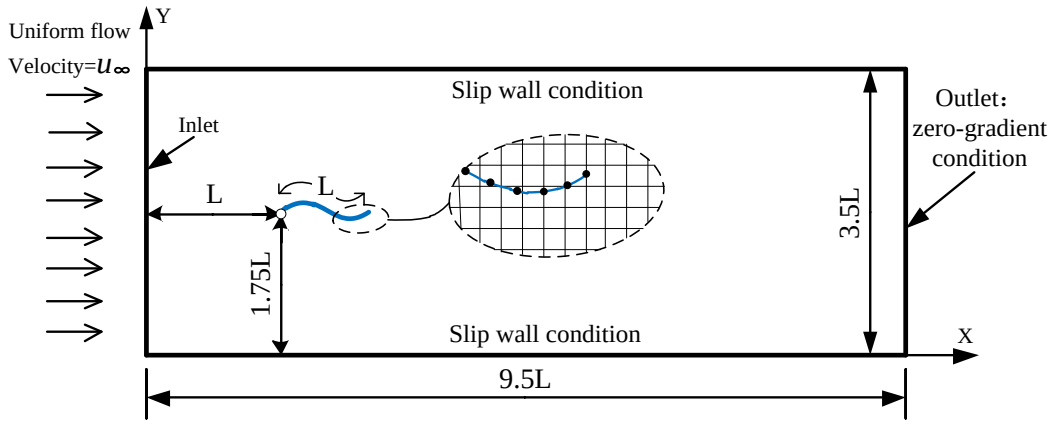

Fig.2. Physical schematic and boundary conditions

According to the references [18-20], the mass of the filament enables the filament to exchange energy with its ambient fluid, and thus plays a significant role in the fluid-filament interaction system. Both of their studies claimed there exist a critical mass density value of M_c,

below which the filament will eventually rest in straight state pointing downstream, while exceed which the filament will enter sustained flapping state. Here, as a validation, 3 cases of dimensionless mass density $M = 0.2, 0.3$ and 0.5, respectively, under $\widehat{K}_s = 50$ ($\widehat{K}_s$ is chosen in a way that the filament is nearly inextensible to ensure the numerical accuracy), $\widehat{K}_b = 10^{-4}$, are studied using our developed IB-LBM algorithm. The vortex structures of the flow field calculated are shown in Fig.3. As we can see, the filament rest in immobile straight state when $M = 0.2$, and keeps flapping when $M = 0.3$ and 0.5. Thus, the critical mass density value of M_c is between $0.2 - 0.3$, which is consistent with the simulation result of Connell and Yue[19], where M_c was predicted to be 0.26 when $Re = 90$. The instantaneous trajectory set of the flapping filament for $M = 0.3$ and 0.5 is presented in Fig.4(a) and Fig.4(b), respectively. Fig.4(c) is the trajectory captured by laboratory experiment[18]. Our simulation result agrees qualitatively well with Zhang's experimental results that the trajectory set of the free end point of the filament appears in a shape of "8" if M exceeds M_c.

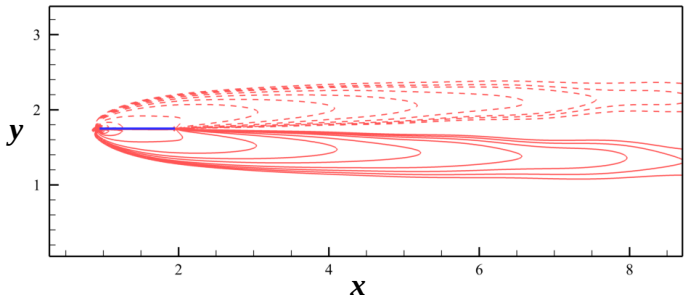

(a) $M = 0.2$

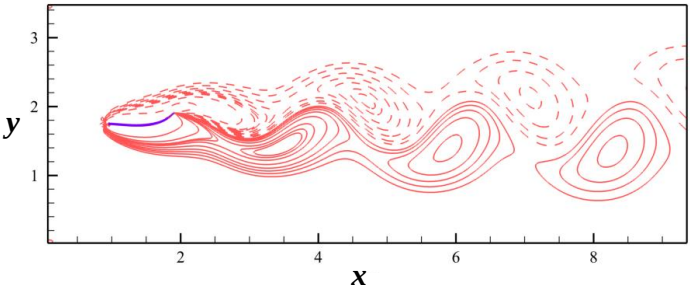

(b) $M = 0.3$

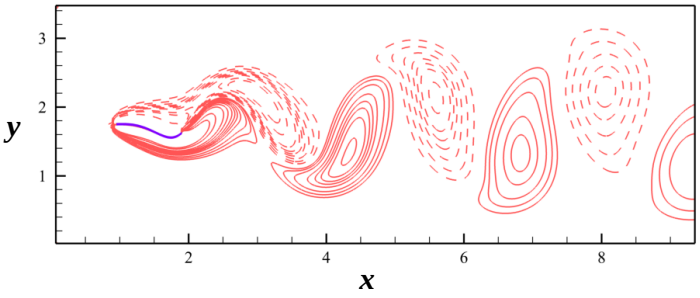

(c) $M = 0.5$

Fig.3. Vortex structures for different mass densities M at $Re = 90,\ Ut/L = 150$.

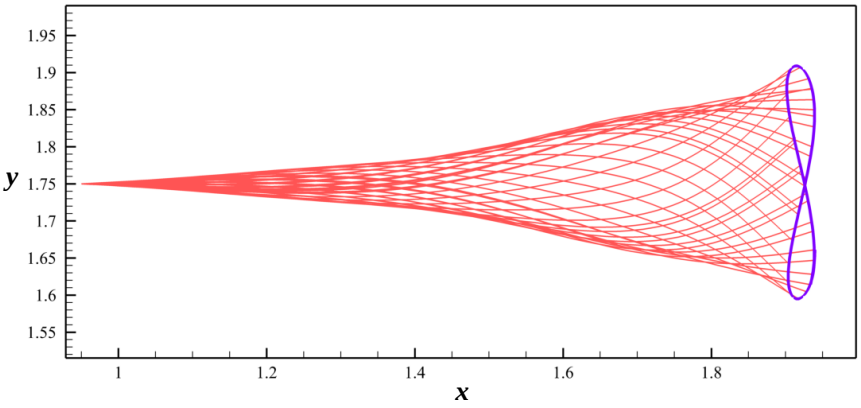

(a) $M = 0.3,\ Re = 90$

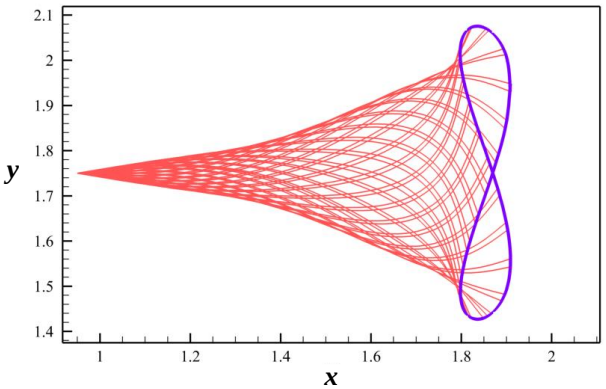

(b) $M = 0.5,\ Re = 90$

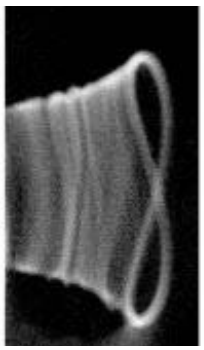

(c) Zhang's experiment

Fig.4. The trajectory set of the flapping filament (orange) and free end point (purple).

3.2 Grid independence and convergence analysis

In order to make sure that our current algorithm is stable and convergent for fluid-flexible-structure-interaction problems, a single filament flapping in a uniform flow is simulated with four different grid sizes Δx, at $Re = 90,\ M = 0.3,\ \widehat{K}_s = 50,\ \widehat{K}_b = 10^{-4}$ and Lagrangian grid space $\Delta s = \Delta x$. The maximum amplitude A, and drag coefficient C_d are calculated and make comparison using the following formulas,

$$A = \max(Y_i) - \min(Y_i), \tag{26}$$

$$C_d = \frac{\sum_i F_x(\vec{X}_i)\Delta s}{0.5\rho\left(u_\infty\right)^2 L},\quad \mathrm{i} = 0, 1, \cdots, \mathrm{Nb} \tag{27}$$

where Y_i is the y-component of position vector $\vec{X}_i$, $F_x(\vec{X}_i)$ is the hydrodynamic force exerted on the boundary point in x-direction, Δs is the grid space for the filament, and L is the length of the filament.

The numerical result is tabulated in Table 1. From the table, we can see both of the two

quantities convergent as the grid get refined, and a grid size of $\Delta s \leq 1/100$ would be small enough considering the limited accuracy improvement during grid refinement process and the increased computational cost.

Table 1. Then comparison of A and C_d under different grid sizes

Δx	A	C_d
$1/50$	0.384	0.422
$1/70$	0.356	0.421
$1/100$	0.343	0.419
$1/140$	0.331	0.419

4. The FSI solver's application on fiber conveyance

4.1 Physical model and boundary conditions

The physical model of our target problem is a two-dimensional trapezoidal channel $(6L \times 2L)$ with a certain conical degree, which is demonstrated in Fig.4, where α is the angle of inclination of the walls. Under current IB-LBM frame, the equation of the upper wall can be determined as $l1: y = \tan\alpha \cdot x$, and the bottom wall as $l2: y = -\tan\alpha \cdot x + 2L$. Therefore, the conical degree of FTC, which is characterized by $tan\alpha$ in this study, can be altered by changing the value of the angle α.

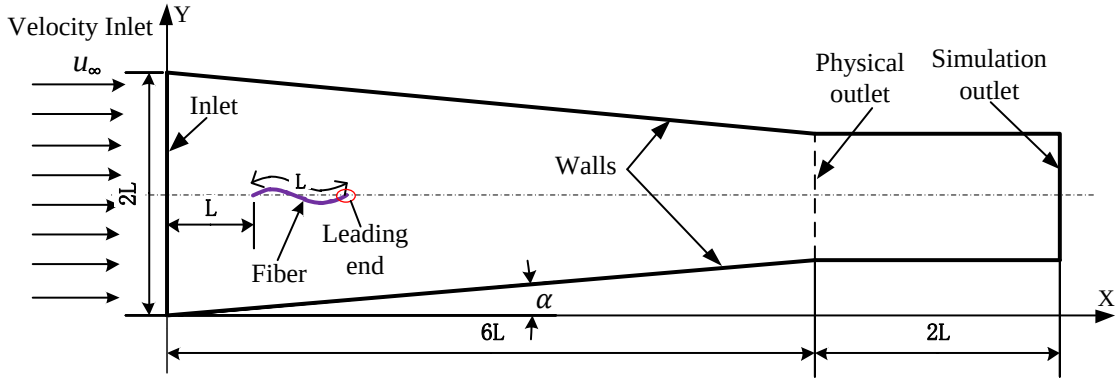

Fig.5. Schematic view of the problem

As shown in Fig.4, an incompressible airflow with a constant velocity profile u_∞ enters the trapezoidal channel to deliver a slender fiber (length= L) whose upstream end is initially

positioned at (L, L). A bounce-back scheme is applied to the upper and bottom walls to satisfy the no-slip boundary condition and the physical outlet is extended to make the flow fully developed, where at the outlet the zero-gradient condition is imposed. As both the upstream end and downstream end of the slender fiber are set free during conveyance, the free-end boundary condition (as described in Eq. (29)) is applied to those ends. Note that the conveyance simulation terminates when any of the fiber nodes reaches the physical outlet.

In each of the following simulations, the fiber's parameters are non-dimensionalized as in section 3.1, and $\widehat{K}_s = 50,\ \Delta s = \Delta x = 1/100$ (which means there are 101 Lagrangian points covering the fiber, i.e. Nb=101), is used in all cases to make the fiber nearly inextensible and the algorithm computationally stable and convergent. The fiber is initially (t =0) at equilibrium state at the center line of FTC and given with a wavy configuration (the coordinates of fiber nodes conform to a sine function with an amplitude of $0.1L$), which is the most common one in cotton fibers.

4.2 Results and discussion

4.2.1 Fiber straightness and leading angle evaluation

To characterize the straightness and leading orientation of the fiber during conveyance, two parameters $\emptyset$ and θ are proposed in this study, as depicted in Fig.5. The first and the last fiber nodes are connected up into Line l The angle between Line l and horizontal direction defines the leading angle θ which characterize the fiber orientation. The summation of distance h_k^2 characterize the fiber straightness $\emptyset$, where h_k is the distance of fiber node k to its foot point on Line l.

$$\emptyset = \sum_{i=0}^{Nb} h_i^2 \tag{28}$$

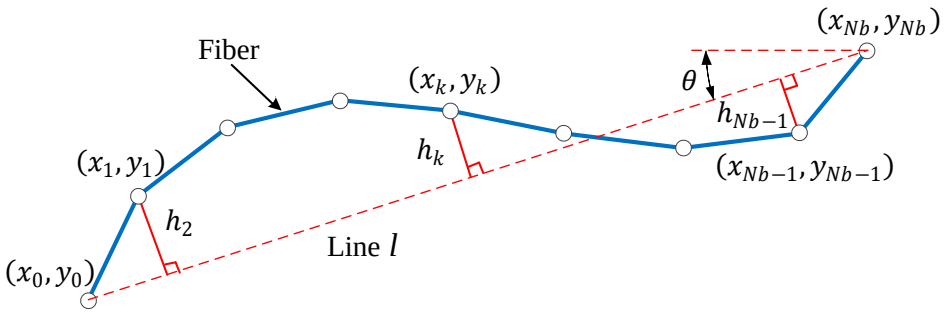

Fig.6. Fiber straightness $\emptyset$ and leading angle θ

According to the definition of straightness $\emptyset$, it's easy to make the conclusion that a smaller value of $\emptyset$ denotes a straighter fiber and a smaller θ means a more horizontal orientation. Note that in textile industry, normally a smaller $\emptyset$ and θ are more desirable during fiber conveyance process, which is considered to be good to the following yarn-forming process.

4.2.2 Effect of the conical degree of FTC on fiber conveyance

It is widely acknowledged that the converging-shape FTC is helpful to accelerate the fiber and straighten their orientations. In this section, numerical study was carried out to investigate how the conical degree of FTC affects fiber motion and whether the converging shape of FTC improves the straightness of the fiber. To satisfy the desired cross-sectional area for conveyance (an excessively narrow FTC will dramatically increase the possibility of fiber-wall collision which may lower the transport efficiency instead), the cases including $\tan\alpha$ =0, $1/20$, $1/15$ and $1/12$, are simulated using present FSI algorithm.

Fig.7 shows the conveyance of a slender fiber in FTCs with different conical degrees, and one of its instantaneous velocity and vortex contours are exhibited in Fig.8. According to Fig.7, the fiber does not maintain its initial equilibrium wavy configuration but deforms and deviates during its conveyance in FTC. The evolution of fiber straightness and leading angle during its conveyance in FTCs with different conical degrees are shown in Fig.9 and Fig.10, respectively. Note that the time step t is scaled by the far-field velocity U and the fiber length L. It can be seen in these figures that it takes FTC with a larger conical degree longer to deliver the fiber to the exit of FTC, which seems to conflict with our common belief that a more converging shape will always be more efficient in fiber delivery. One possible explanation for this is that, when the conical degree of the FTC is increased, the fiber is more streamlined (i.e. with a small leading angle, see Fig.10), and has a smaller frontal area during conveyance. This reduces the overall drag exerted on the fiber as the dominate pressure drag is greatly reduced, though the friction drag may increase. Consequently, the fiber conveyance speed and delivery efficient is decreased. Moreover, the figure in Fig.8 indicates that the fiber's straightness increases radically at the first 1/5 conveyance process and then drops rapidly to the value around 0 (which

means an almost straight configuration) for all conical degrees. After that, the trend for different α starts to go separate ways. That is, for FTCs with no conical degree ($\tan\alpha$=0), the fiber straightness keeps increasing all the way to the exit, while for FTCs with a certain conical degree, the straightness experience an rise-decline trend similar to previous. The evolution of fiber leading angle is much simpler. As can be seen in Fig.10, after a slightly adjust at the beginning, the fiber leading angle for all cases increases to its maximum in the first half stage and then declines in the second half stage. And the fluctuation is more severe in FTCs with a smaller $\tan\alpha$, this conclusion is also applicable in the trend of straightness. The exceptional case of $\tan\alpha = 1/20$ occurs may be due to the influence of fiber-wall contact, which brings a larger fiber deformation at the last 1/3 process. Therefore, conclusions can be drawn that the FTC with a converging shape is useful to straighten fiber and adjust its orientation, and a larger conical degree brings a better straighten effect and a smaller leading angle if fiber-wall contact does not occur.

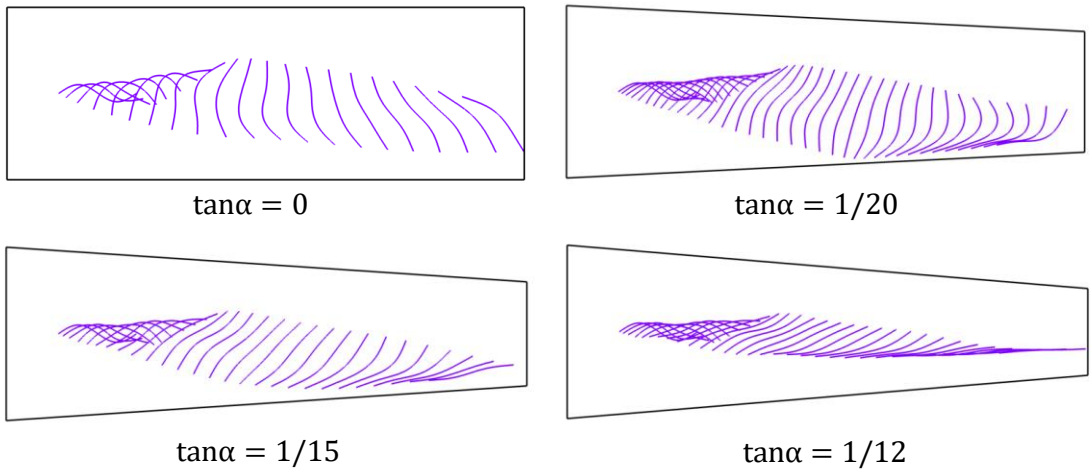

Fig.7. The conveyance of a slender fiber in FTCs with different conical degrees $\tan\alpha$ (Time interval $U\Delta t/L = 0.8, \hat{K}_b = 5 \times 10^{-4}, Re = 400$)

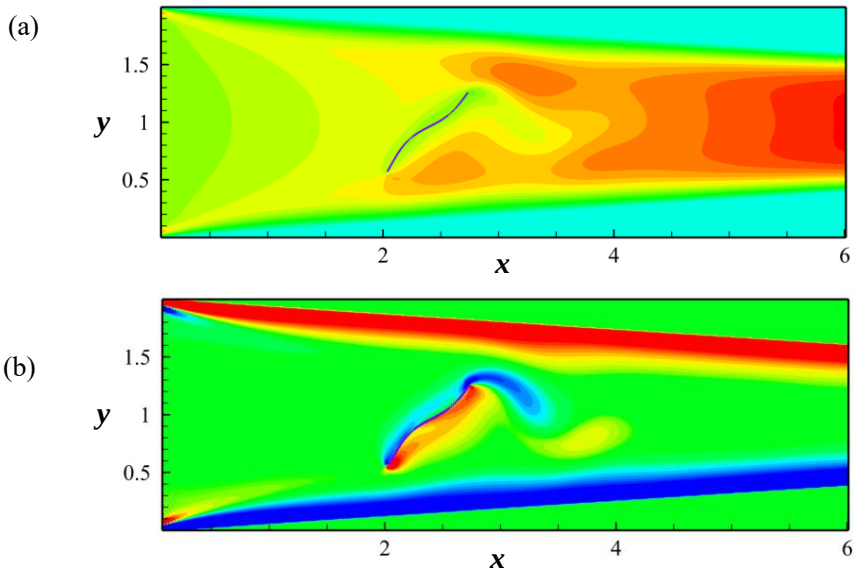

Fig.8. The instantaneous velocity (a) and vortex (b) contours during conveyance ($Ut/L = 6.8$, $\tan\alpha = 1/15$, $\widehat{K}_b = 5 \times 10^{-4}$, $Re = 400$)

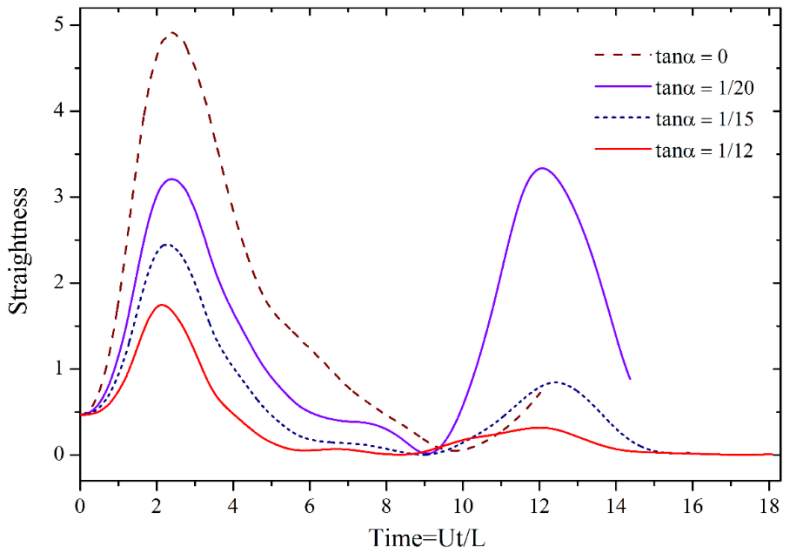

Fig.9. The evolution of fiber straightness during its conveyance in FTCs with different conical degrees ($\widehat{K}_b = 5 \times 10^{-4}$, $Re = 400$)

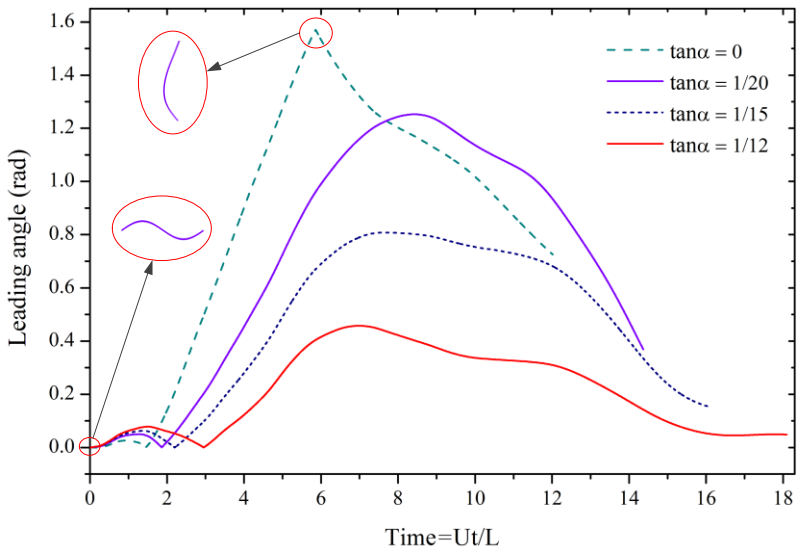

Fig.10. The evolution of fiber leading angle during its conveyance in FTCs with different conical degrees ($\widehat{K}_b = 5 \times 10^{-4}, Re = 400$)

4.2.3 Effect of the fiber bending rigidity on fiber conveyance

The flexibility of fiber is characterized by the bending rigidity, and a smaller bending rigidity means a more flexible fiber. In this part, the effect of dimensionless bending rigidity $\widehat{K}_b$ on fiber conveyance in a trapezoidal FTC with a conical degree of $\tan\alpha = 1/15$ and $Re = 400$ is investigated. The snapshots in Fig.11 provides the trajectories of fiber with various bending rigidities during its conveyance in FTC. As we can see, the fiber is transported in a more horizontal direction (closer to the center line of FTC) in the cases of $\widehat{K}_b = 1 \times 10^{-4}$ and $\widehat{K}_b = 1 \times 10^{-3}$. The evolution of fiber straightness and leading angle are plotted in Fig.12 and Fig.13, respectively. As we can see, the trends displayed in these two figures are similar to the case regarding conical degrees that the straightness follows a "leap-slump-grow-drop" evolution process and the leading angle follows an "increase-decline" trend for fibers with a smaller bending rigidity. However, as $\widehat{K}_b$ keeps increasing to 1×10^{-3}, there is no "grow-drop" trend for straightness to appear in the second half conveyance. Actually, the fiber is delivered in an almost straight and horizontal orientation (both $\emptyset$ and θ are close to 0), despite some small fluctuations. Apart from that, conclusions can be drawn from Fig.12 and Fig.13 by making comparison between different $\widehat{K}_b$, that the bending rigidity have a significant effect on fiber configuration and orientation during its conveyance, and a fiber with a larger bending

rigidity is more likely to maintain a straighter configuration and a more horizontal orientation.

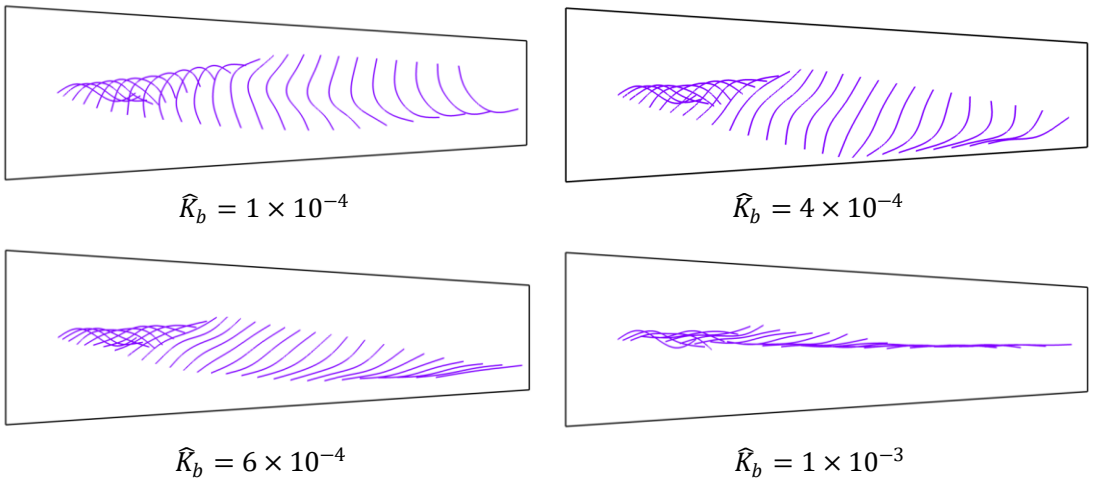

Fig.11. The conveyance of a slender fiber with different bending rigidities in FTC (Time interval $U\Delta t/L = 0.8, \tan\alpha = 1/15, Re = 400$)

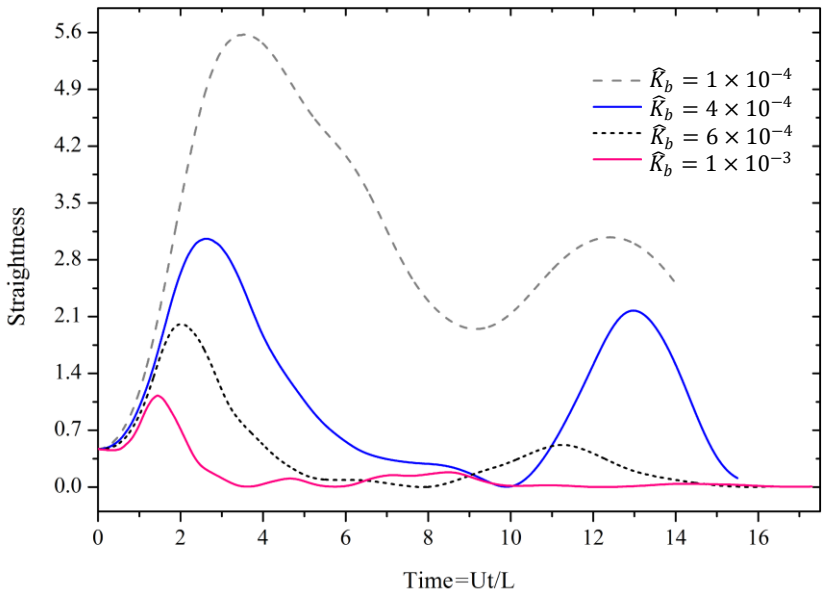

Fig.12. The evolution of fiber straightness during its conveyance in FTCs with different bending rigidities ($\tan\alpha = 1/15, Re = 400$)

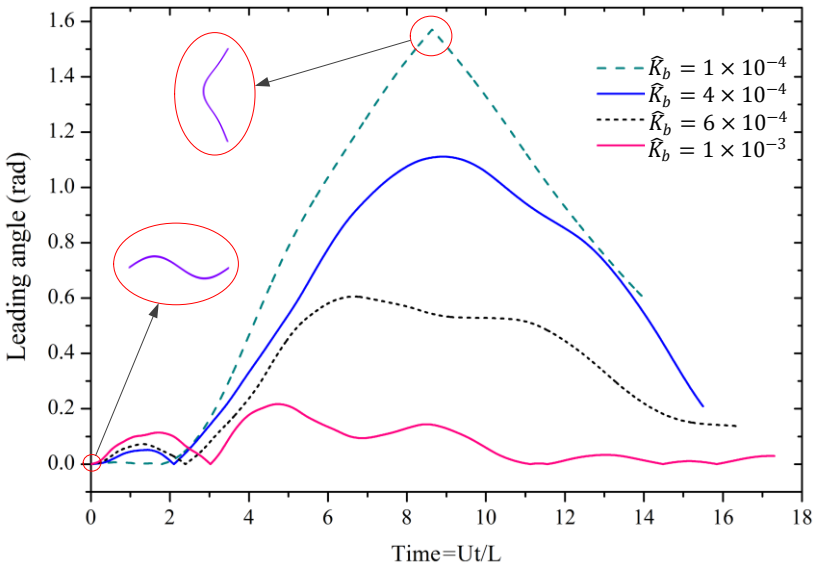

Fig.13. The evolution of fiber leading angle during its conveyance in FTCs with different bending rigidities ($\tan\alpha = 1/15, Re = 400$)

4.2.4 Effect of the flow Reynolds number on fiber conveyance

In pneumatic conveying, the fluid flow plays a very important role for it not only acts as the transportation medium, but also provides the drag force and exerts momentum to the immersed target. In this part, the flow condition's influence on fiber conveyance is numerically studied. A slender fiber's delivery in flows of 4 different Reynolds numbers (Re) are simulated. The fiber's trajectories during conveyance in different flow conditions are presented in Fig.14. From which we can see that as Re increases, the fiber deviates more from the horizontal path to a direction pointing the lower right corner of FTC during conveyance. Fig.15 and Fig.16 plot the straightness and leading angle of fiber versus time, respectively. The trends in these two figures follow the patterns in the previous cases. The figure difference between different cases in this part indicates that as Re increases, both the straightness and leading angle of fiber increases, in other words, the fiber deformation gets larger and the orientation becomes more vertical.

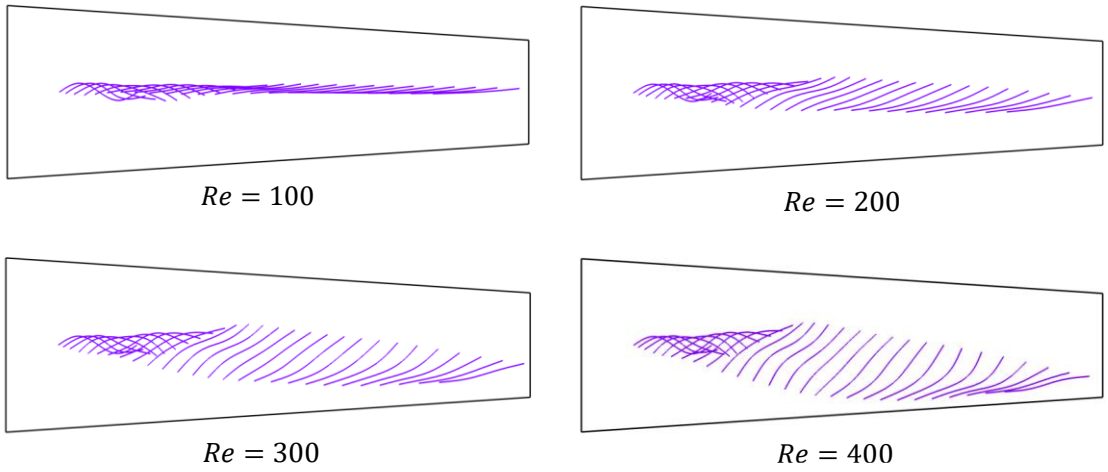

Fig.14. The conveyance of a slender fiber in FTC under different Re (Time interval $U\Delta t/L = 0.8, \tan\alpha = 1/15, \widehat{K}_b = 5 \times 10^{-4}$)

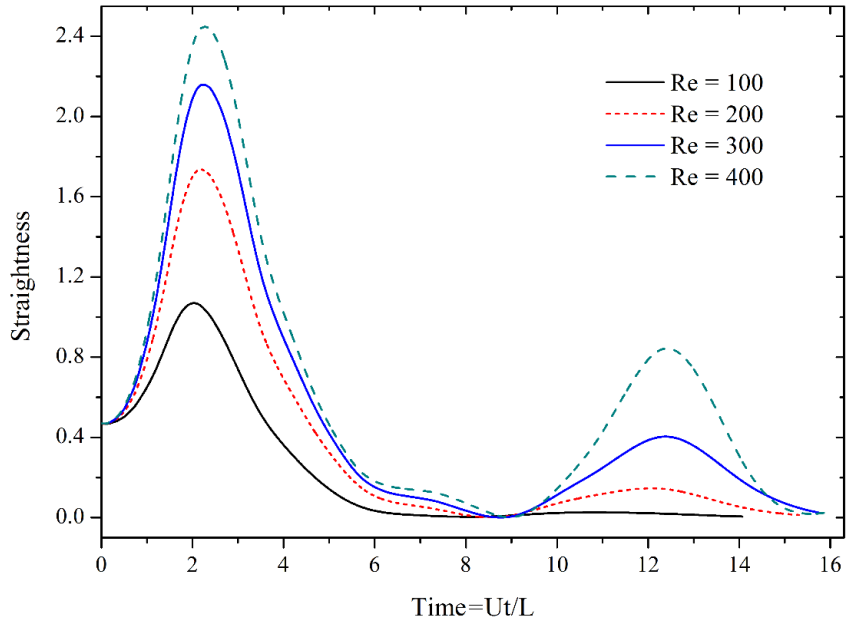

Fig.15. The evolution of fiber straightness during its conveyance in FTC under different Re ($\tan\alpha = 1/15, \widehat{K}_b = 5 \times 10^{-4}$)

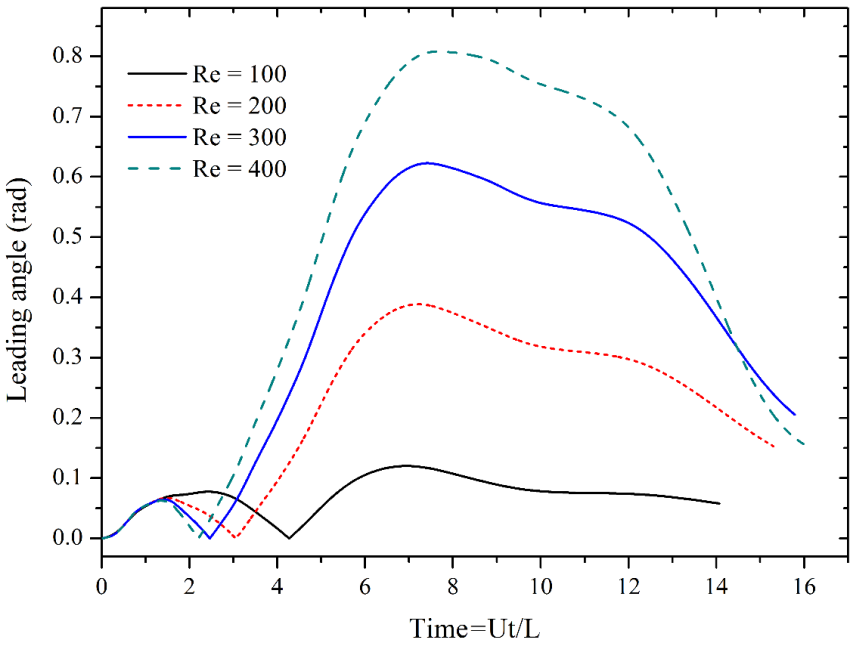

Fig.16. The evolution of fiber leading angle during its conveyance in FTCs under different Re ($\tan\alpha = 1/15, \widehat{K}_b = 5 \times 10^{-4}$)

5 Conclusions

In this paper, a computationally efficient non-body-fitted numerical method for airflow-fiber coupling is developed, namely, the momentum exchange based immersed boundary-lattice Boltzmann method (IB-LBM), to study flexible fiber's conveyance characteristics in confined channel in low-Reynolds-number flow conditions. Numerical simulation on the delivery of a single fiber in a fiber transport channel (FTC) is carried out. Three parameters, the conical degree of the FTC, the bending rigidity of fiber and the flow Reynolds number (Re), on the fiber conveyance are particularly investigated, and some conclusions on fiber conveyance in low-Reynolds-number flows are drawn as follows:

1). IB-LBM based on non-body-fitted grid, can efficiently simulate the interaction between fluid and flexible body that involves large deformation, thus is appropriate to be applied to the pneumatic-type textile field.

2). The converging shape of FTC helps to straighten fiber and adjust its orientation to a more horizontal degree in fiber conveyance, however, it may not improve fiber delivery efficiency due to the reduced pressure drag, and a larger conical degree brings a better straighten effect and a smaller leading angle if fiber-wall contact does not occur.

3). Under the conditions that $\tan\alpha > 0$, $Re < 400$ and $\widehat{K}_b < 1e-3$, the fiber straightness and leading angle experience similar trends among different cases, that is, the straightness undergoes a “leap-slump-grow-drop” evolution process and the leading angle follows an “increase-decline” tendency.

4). The bending rigidity have a significant effect on fiber configuration and orientation during its conveyance, and a fiber with a larger bending rigidity is more likely to maintain a straighter configuration and a more horizontal orientation during its conveyance in low-Reynolds-number flows.

5). The fiber gets less straight in configuration, more vertical in orientation and deviate more from the horizontal path as Reynolds number increases.

6 Acknowledgements

The work was supported by National Natural Science Foundation of China under Grant No.51576180.

7 References

[1] L. X. Kong and R. A. Platfoot, "Fibre transportation in confined channel with recirculations," *Computers & Structures,* Article; Proceedings Paper vol. 78, no. 1-3, pp. 237-245, Nov 2000.

[2] C. A. Lawrence and K. Z. Chen, "A study of the fiber-transfer-channel design in rotor-spinning .1. The fiber trajectory," *Journal of the Textile Institute,* Article vol. 79, no. 3, pp. 367-392, 1988.

[3] C. A. Lawrence and K. Z. Chen, "A study of the fiber-transfer-channel design in rotor-spinning .2. Optimization of the transfer-channel design," *Journal of the Textile Institute,* Article vol. 79, no. 3, pp. 393-408, 1988.

[4] Y. Z. Jin, J. Y. Cui, X. D. Li, and H. L. Chen, "An investigation on the distribution of massive fiber granules in rotor spinning units," *Textile Research Journal,* Article vol. 87, no. 7, pp. 865-877, May 2017.

[5] L. X. Kong and R. A. Platfoot, "Computational two-phase air/fiber flow within transfer channels

of rotor spinning machines," *Textile Research Journal,* Article vol. 67, no. 4, pp. 269-278, Apr 1997.

[6] Z. G. Pei and C. W. Yu, "Numerical study on the effect of nozzle pressure and yarn delivery speed on the fiber motion in the nozzle of Murata vortex spinning," *Journal of Fluids and Structures,* Article vol. 27, no. 1, pp. 121-133, Jan 2011.

[7] C. S. Peskin, "Numerical analysis of blood flow in the heart," *Journal of Computational Physics,* vol. 25, no. 3, pp. 220-252, 1977/11/01/ 1977.

[8] C. S. Peskin, "The fluid-dynamics of heart-valves - experimental, theoretical, and computational methods," *Annual Review of Fluid Mechanics,* Review vol. 14, pp. 235-259, 1982.

[9] C. S. Peskin, "The immersed boundary method," *Acta Numerica,* vol. 11, pp. 479-517, 2003.

[10] C. D. Eggleton and A. S. Popel, "Large deformation of red blood cell ghosts in a simple shear flow," *Physics of Fluids,* Article vol. 10, no. 8, pp. 1834-1845, Aug 1998.

[11] L. J. Fauci and A. McDonald, "Sperm motility in the presence of boundaries," *Bulletin of Mathematical Biology,* Article vol. 57, no. 5, pp. 679-699, Sep 1995.

[12] L. J. Fauci and C. S. Peskin, "A computational model of aquatic animal locomotion," *Journal of Computational Physics,* Article vol. 77, no. 1, pp. 85-108, Jul 1988.

[13] L. A. Miller and C. S. Peskin, "When vortices stick: an aerodynamic transition in tiny insect flight," *Journal of Experimental Biology,* Article vol. 207, no. 17, pp. 3073-3088, Aug 2004.

[14] S. Chen and G. D. Doolen, "Lattice boltzmann method for fluid flows," *Annual Review of Fluid Mechanics,* vol. 30, no. 1, pp. 329-364, 1998/01/01 1998.

[15] K. Vahidkhah and V. Abdollahi, "Numerical simulation of a flexible fiber deformation in a viscous flow by the immersed boundary-lattice Boltzmann method," *Communications in Nonlinear Science and Numerical Simulation,* Article vol. 17, no. 3, pp. 1475-1484, Mar 2012.

[16] F. B. Tian, H. X. Luo, L. D. Zhu, J. C. Liao, and X. Y. Lu, "An efficient immersed boundary-lattice Boltzmann method for the hydrodynamic interaction of elastic filaments," *Journal of Computational Physics,* Article vol. 230, no. 19, pp. 7266-7283, Aug 2011.

[17] H. Z. Yuan, X. D. Niu, S. Shu, M. J. Li, and H. Yamaguchi, "A momentum exchange-based immersed boundary-lattice Boltzmann method for simulating a flexible filament in an incompressible flow," *Computers & Mathematics with Applications,* Article vol. 67, no. 5, pp. 1039-1056, Mar 2014.

[18] J. Zhang, S. Childress, A. Libchaber, and M. Shelley, "Flexible filaments in a flowing soap film as a model for one-dimensional flags in a two-dimensional wind," *Nature,* Article vol. 408, no. 6814, pp. 835-839, Dec 2000.

[19] B. S. H. Connell and D. K. P. Yue, "Flapping dynamics of a flag in a uniform stream," *Journal of Fluid Mechanics,* Article vol. 581, pp. 33-68, Jun 2007.

[20] L. D. Zhu and C. S. Peskin, "Interaction of two flapping filaments in a flowing soap film," *Physics of Fluids,* Article vol. 15, no. 7, pp. 1954-1960, Jul 2003.

[21] X. D. Niu, C. Shu, Y. T. Chew, and Y. Peng, "A momentum exchange-based immersed boundary-lattice Boltzmann method for simulating incompressible viscous flows," *Physics Letters A,* Article vol. 354, no. 3, pp. 173-182, May 2006.

[22] A. J. C. Ladd, "Numerical simulations of particulate suspensions via a discretized boltzmann-equation .1. Theoretical foundation," *Journal of Fluid Mechanics,* Article vol. 271, pp. 285-309, Jul 1994.

[23] A. J. C. Ladd, "Numerical simulations of particulate suspensions via a discretized boltzmann-equation .2. Numerical results," *Journal of Fluid Mechanics,* Article vol. 271, pp. 311-339, Jul 1994.